

Thin magnetized disk solutions and trends in the angular momentum flux

Miljenko Čemeljić

with W. Kluźniak, V. Parthasarathy

Nicolaus Copernicus Astronomical Center,
Warsaw, Poland

Outline

- Introduction
- Analytical HD disk solution
- Numerical simulations in HD and MHD
- “Atlas” of solutions
- Trends in the angular momentum flux
- Expressions for physical quantities
- Outflows and jets
- Summary

Introduction

- First numerical solution of (HD) accretion disk was by Prendergast & Burbidge (1968)
- Analytical solution was given by Shakura & Sunyaev (1973)
- ... (lots of good things, but mostly with 1D, vertically averaged models)
- In Kluźniak & Kita (2000, KK00) was given a solution of the HD polytropic disk in the full 3D. It was obtained by the method of asymptotic approximation.
- In 2009, numerical simulations of star-disk magnetospheric interaction were done in 2D-axisymmetric simulations, by Romanova et al. (2009, 2013, with non-public code), Zanni & Ferreira (2009, 2013, with publicly available code).
- Development of disk simulations went in the direction of MRI in the disk (Flock et al. 2012) or radiative transfer simulations, but for a decade nothing much happened in star-disk magnetospheric interaction simulations.
- In Čemeljić et al. (2017), with PLUTO code, we reported the first repeating of Zanni et al. (2009, 2013) 2D axisymmetric viscous & resistive MHD simulations.
- A parameter study is now possible, to investigate the influence of different parameters.

Numerical setup

- I perform simulations of a rotating thin accretion disk, which reach a quasi-stationary state.

- Ohmic and viscous heating in the energy equation are neglected, assuming that all the heat is radiated away.

$$\frac{\partial \rho}{\partial t} + \nabla \cdot (\rho \mathbf{u}) = 0$$

$$\frac{\partial \rho \mathbf{u}}{\partial t} + \nabla \cdot \left[\rho \mathbf{u} \mathbf{u} + \left(P + \frac{\mathbf{B} \cdot \mathbf{B}}{8\pi} \right) \mathbf{I} - \frac{\mathbf{B} \mathbf{B}}{4\pi} - \boldsymbol{\tau} \right] = \rho \mathbf{g}$$

- Viscosity and resistivity are still included, in the equation of motion and in the induction equation.

$$\frac{\partial E}{\partial t} + \nabla \cdot \left[\left(E + P + \frac{\mathbf{B} \cdot \mathbf{B}}{8\pi} \right) \mathbf{u} - \frac{(\mathbf{u} \cdot \mathbf{B}) \mathbf{B}}{4\pi} \right] + \nabla \cdot [\eta_m \mathbf{J} \times \mathbf{B} / 4\pi - \mathbf{u} \cdot \boldsymbol{\tau}] = \rho \mathbf{g} \cdot \mathbf{u} - \Lambda_{\text{cool}}$$

$$\frac{\partial \mathbf{B}}{\partial t} + \nabla \times (\mathbf{B} \times \mathbf{u} + \eta_m \mathbf{J}) = 0.$$

- Code I use is PLUTO (v.4.1) by Mignone et al. (2007, 2012).

Initial conditions

Initial conditions are HD disk and a hydrostatic corona. Examples from derivation in KK00.

Equation of continuity:

$$\frac{\epsilon}{r} \frac{\partial}{\partial r} (r \rho v_r) + \frac{\partial}{\partial z} (\rho v_z) = 0 \quad (1)$$

Order ϵ^0 :

$$\frac{\partial}{\partial z} (\rho_0 v_{z0}) = 0 \Rightarrow v_{z0} = 0 \quad (2)$$

Order ϵ^1 :

$$\frac{1}{r} \frac{\partial}{\partial r} (r \rho_0 v_{r0}) + \frac{\partial}{\partial z} (\rho_0 v_{z1}) = 0 \quad (3)$$

From the argumentation presented below, for the first order in ϵ of the radial momentum, we have $v_{r0} = 0$, so that here we have $\partial_z(\rho_0 v_{z1}) = 0 \Rightarrow \rho_0 v_{z1} = \text{const}$ along z . Since v_z is odd with respect to z , at the disk equatorial plane it is $\rho_0 v_{z1} = 0$. Since it does not depend on z , and $\rho_0 \neq 0$, we conclude that $v_{z1} = 0$.

Order ϵ^2 :

$$\frac{1}{r} \frac{\partial}{\partial r} (r \rho_0 v_{r1}) + \frac{\partial}{\partial z} (\rho_0 v_{z2}) = 0 \quad (4)$$

Vertical momentum:

$$\begin{aligned} \epsilon v_r \frac{\partial v_z}{\partial r} + v_z \frac{\partial v_z}{\partial z} = & -\frac{z}{r^3} \left[1 + \epsilon^2 \left(\frac{z}{r} \right)^2 \right]^{-3/2} \\ -n \frac{\partial c_s^2}{\partial z} + \frac{2}{\gamma \tilde{\beta}} \frac{1}{\rho} \left(\epsilon B_r \frac{\partial B_z}{\partial r} + B_z \frac{\partial B_z}{\partial z} \right) - \frac{1}{\gamma \tilde{\beta}} \frac{1}{\rho} \frac{\partial B^2}{\partial z} \\ & + \frac{2}{\rho} \frac{\partial}{\partial z} \left(\eta \frac{\partial v_z}{\partial z} \right) + \frac{\epsilon^2}{\rho r} \frac{\partial}{\partial r} \left(r \eta \frac{\partial v_z}{\partial r} \right) \\ & - \frac{2}{3} \frac{\epsilon}{\rho} \frac{\partial}{\partial z} \left(\frac{\eta}{r} \frac{\partial}{\partial r} (r v_r) \right) - \frac{2}{3\rho} \frac{\partial}{\partial z} \left(\eta \frac{\partial v_z}{\partial z} \right) \\ & + \frac{\epsilon}{\rho r} \frac{\partial}{\partial r} \left(\eta r \frac{\partial v_r}{\partial z} \right) \end{aligned} \quad (17)$$

Order ϵ^0 :

$$0 = -\frac{z}{r^3} - n \frac{\partial c_{s0}^2}{\partial z} - \frac{1}{\gamma \tilde{\beta}} \frac{1}{\rho_0} \frac{\partial B_0^2}{\partial z} \quad (18)$$

Since we had $\partial B_{r0}/\partial z = \partial B_{z0}/\partial z = \partial B_{\varphi 0}/\partial z = 0$, we have $\partial B_0/\partial z = 0$, i.e. $B_0 = f(r)$. We have then

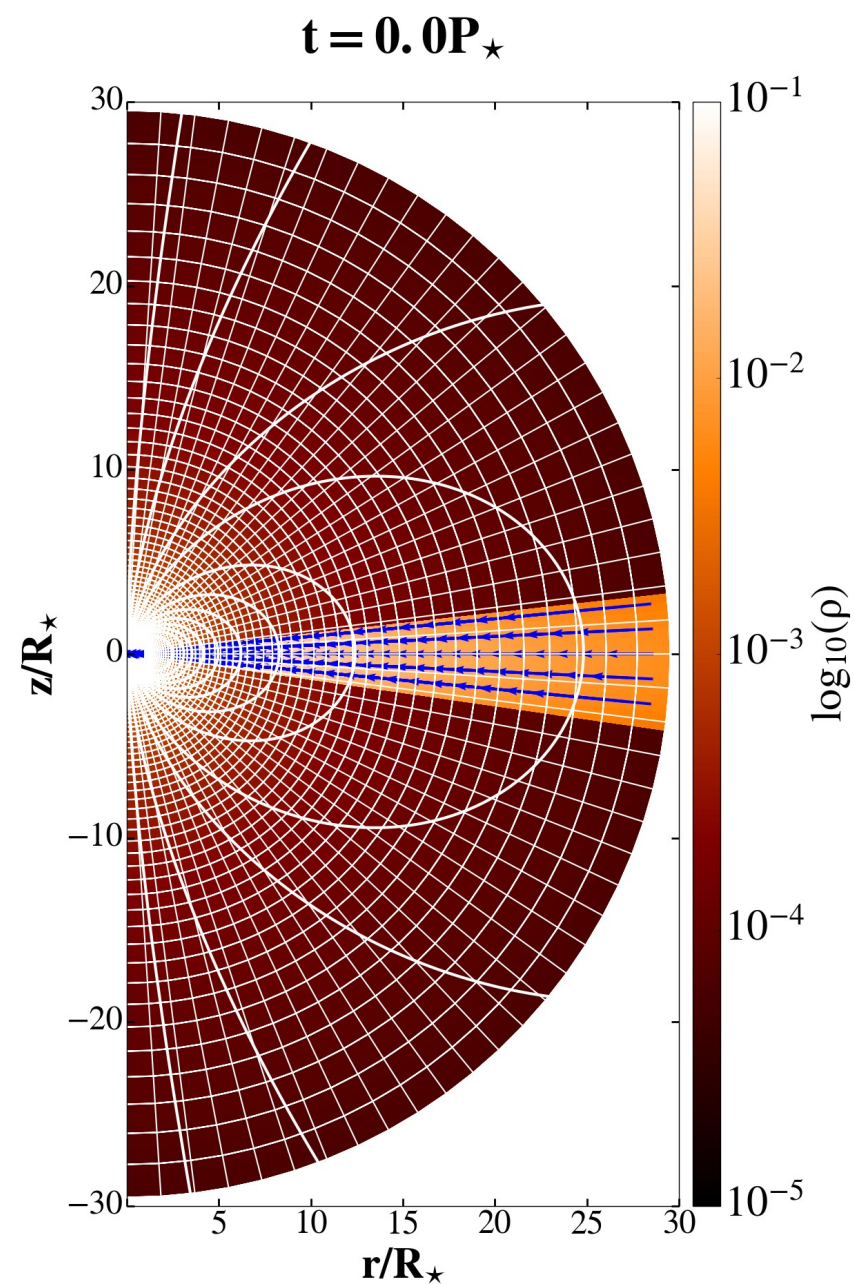
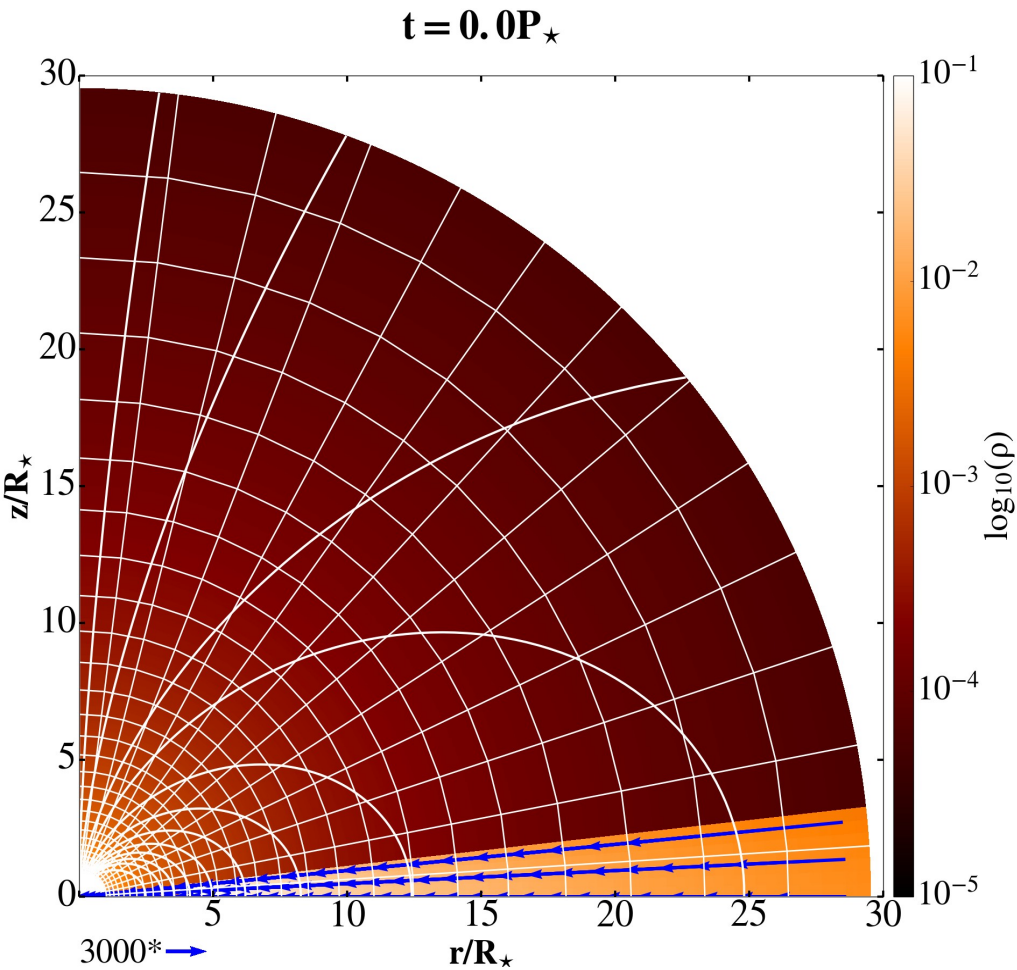
$$\frac{z}{r^3} = -n \frac{\partial c_{s0}^2}{\partial z}, \quad (19)$$

which is the vertical hydrostatic equilibrium equation, with the solution in the case of $n = 3/2$:

$$c_{s0} = \sqrt{\frac{h^2 - z^2}{3r^3}}, \quad \rho_0 = \left(\frac{h^2 - z^2}{5r^3} \right)^{3/2}, \quad (20)$$

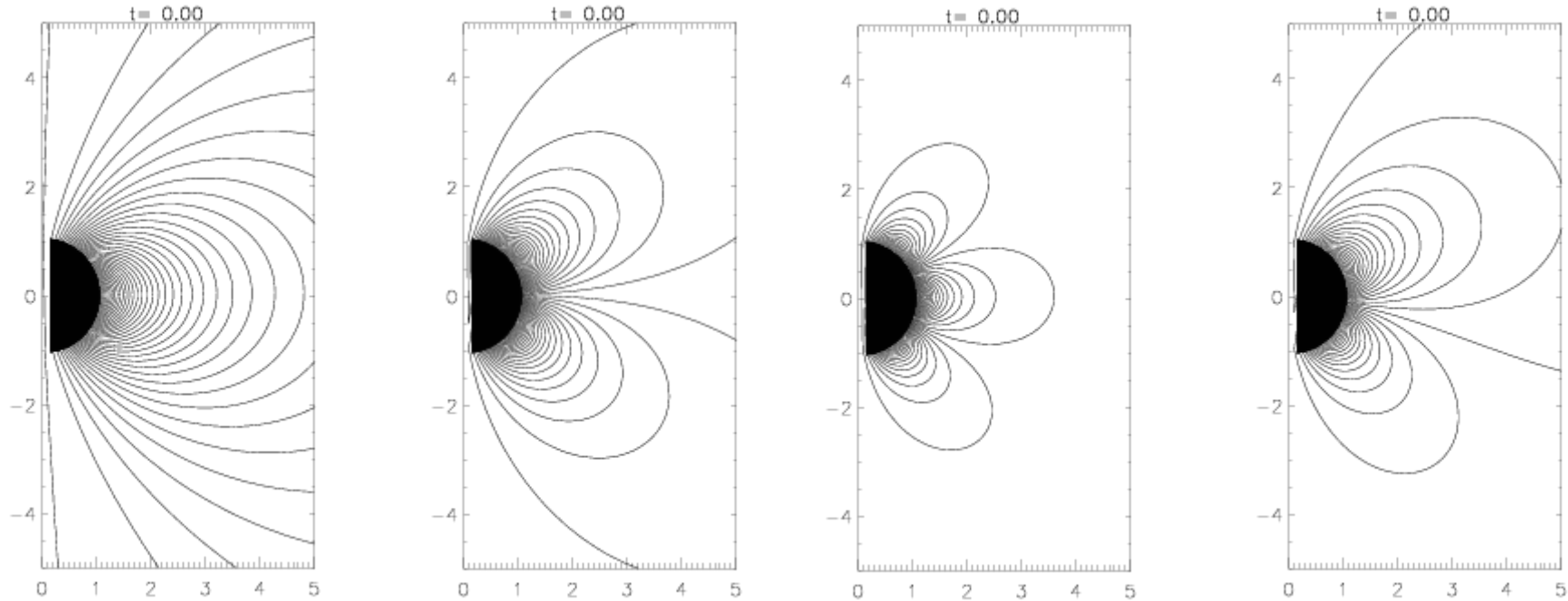
where h is the semi-thickness of the disk. This also gives us the pressure relation $P = \rho_0^{5/3} = [(h^2 - z^2)/5r^3]^{5/2}$ (Hoshi 1977; Kluźniak & Kita 2000).

Star-disk simulations setup



- We add the magnetic field to the HD solution
- Stellar surface is a rotating boundary condition at the origin of the spherical computational domain. We assume the star to be a solid magnetized rotator. The initially non-rotating corona is in a hydrostatic balance.

Star-disk simulations setup



- I add the stellar dipole field to the KK00 solution. Simulations with quadrupole, octupole and multipole field were also performed.

Star-disk simulations setup

Table 1. The parameters in our study presented in the “Atlas”: the stellar angular velocity Ω_\star , stellar dipole magnetic field strength B_\star , and the magnetic Prandtl number P_m -for which we also table the values of corresponding resistivity coefficient α_m . We show also the stellar rotation period, and corotation radius in young stellar object (YSO) cases.

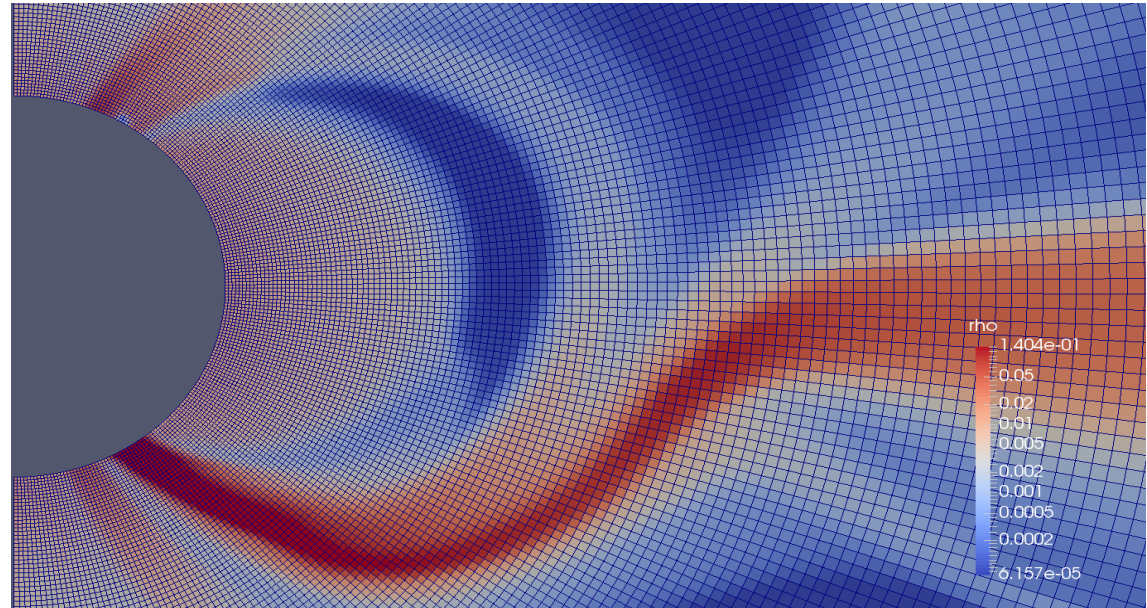
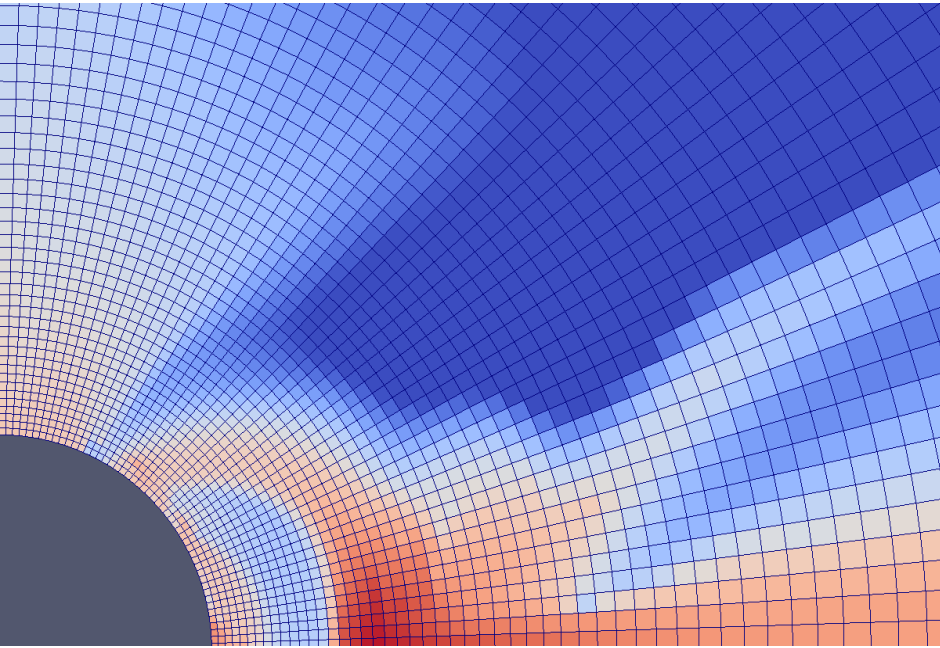
$\Omega_\star/\Omega_{\text{br}}$	$B_\star(\text{G})$	P_m	α_m	$P_\star(\text{days})$	$R_{\text{cor}}(R_\star)$
0.05	250	6.7	0.1	9.2	7.37
0.1	500	1.67	0.4	4.6	4.64
0.15	750	0.95	0.7	3.1	3.54
0.2	1000	0.67	1.0	2.3	2.92

- I did a systematic study with magnetic star-disk numerical simulations in 64 points in parameter space, for a slowly rotating star, with $\alpha_v=1$.
- Prandtl magnetic number:

$$P_m = \frac{2}{3} \frac{\alpha_v}{\alpha_m}$$

Star-disk simulations setup

- Two kinds of simulations in 2D-axisymmetric grid:



$R \times \vartheta = [217 \times 100]$ grid cells in $\vartheta = [0, \pi/2]$

$R \times \vartheta = [217 \times 1200]$ grid cell in $\vartheta = [0, \pi]$

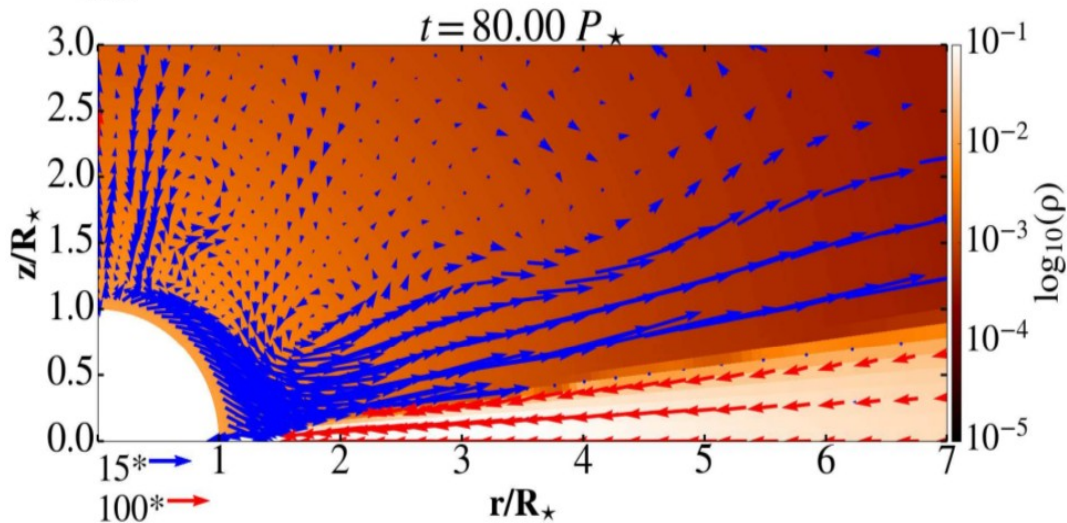
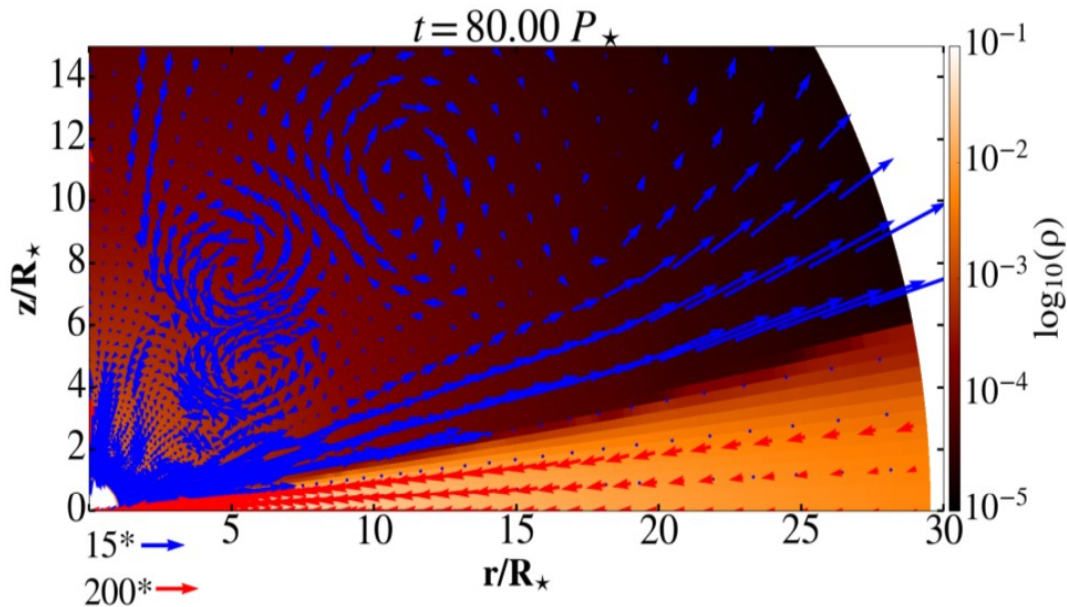
Logarithmic grid spacing in the radial, and uniform spacing in the latitudinal direction.

Star rotates at about 1/10 of the breakup rotational velocity.

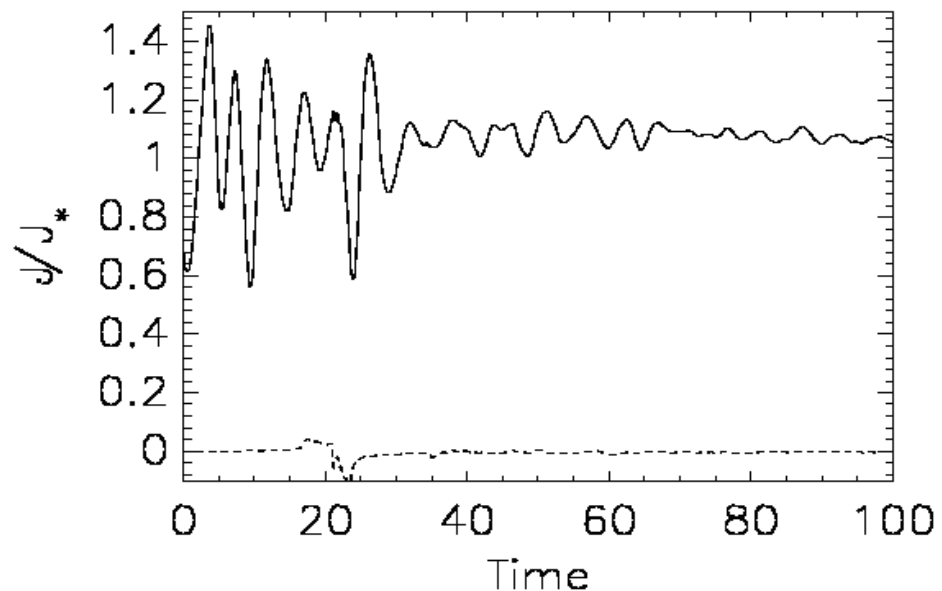
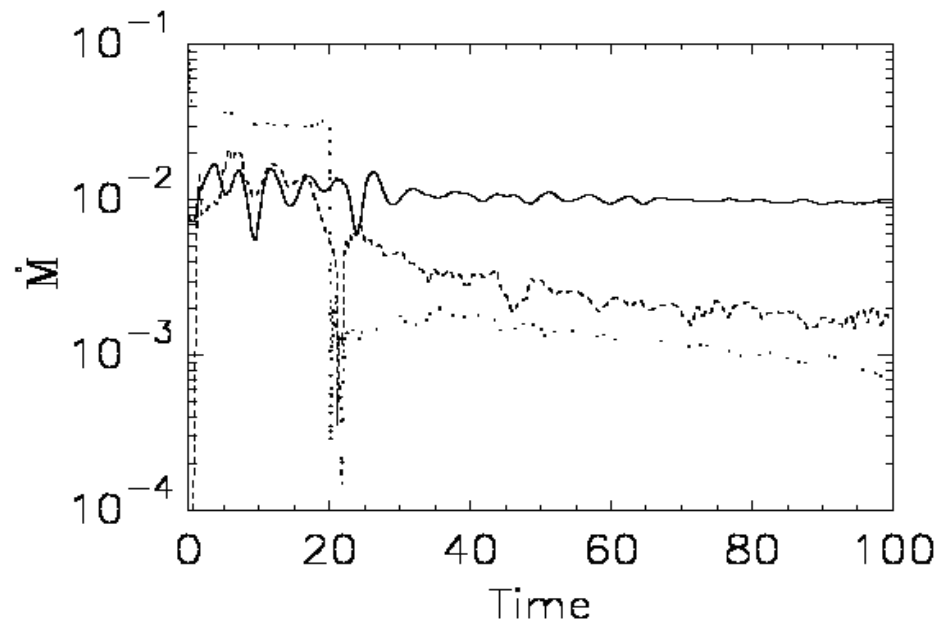
Mass and angular momentum fluxes : $\dot{M} = \int_S \rho \mathbf{v}_p \cdot d\mathbf{S}$, $\dot{J} = \int_S \left(r \rho v_\varphi \mathbf{v}_p - \frac{r B_\varphi \mathbf{B}_p}{4\pi} \right) d\mathbf{S}$

Units of stellar angular momentum expressed in: $J_{\star 0} = \rho_{d0} R_\star^4 V_{K\star}$

Hydro-dynamical star-disk simulations

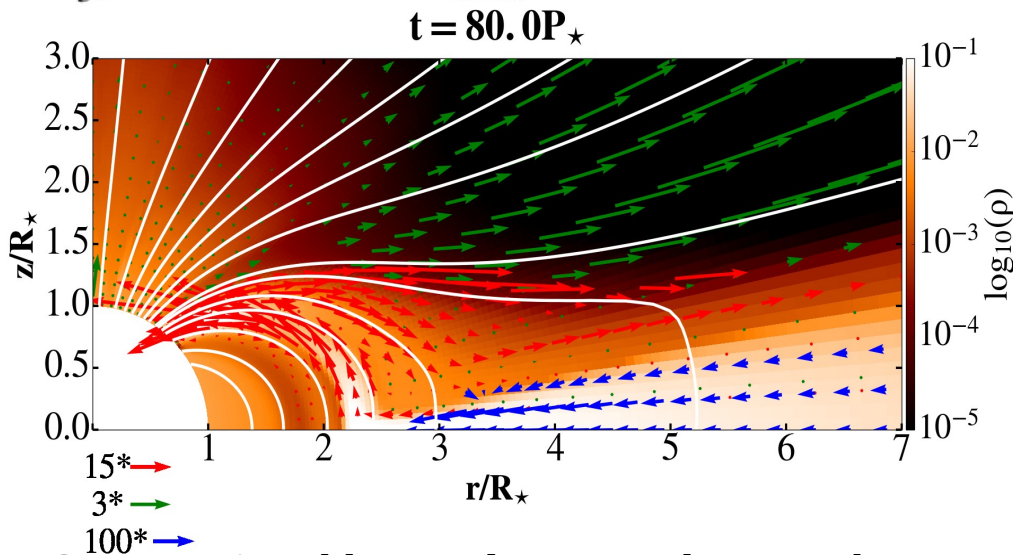
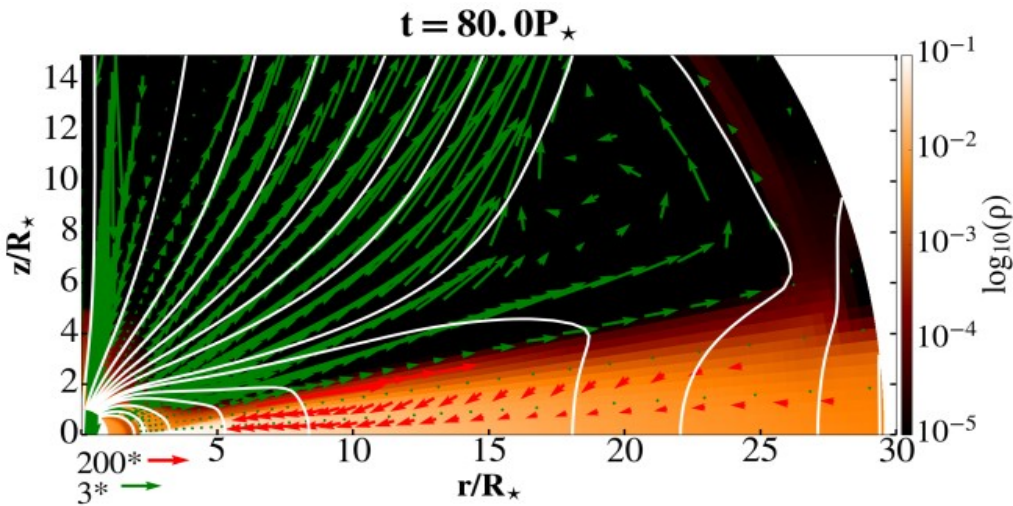


Computational box and a zoom closer to the star after 80 stellar rotations. In color is shown the density, and vectors show velocity, with the different normalization in the disk and stellar wind.

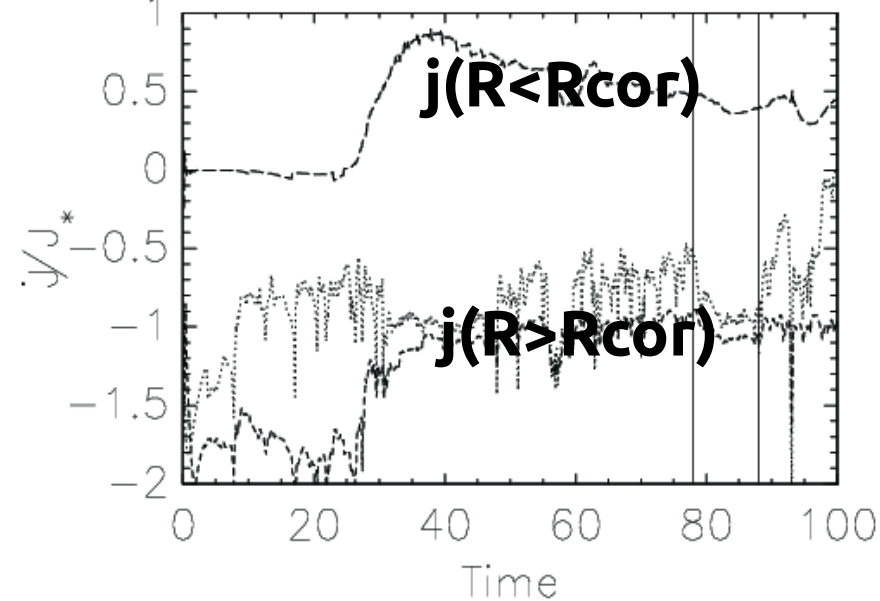
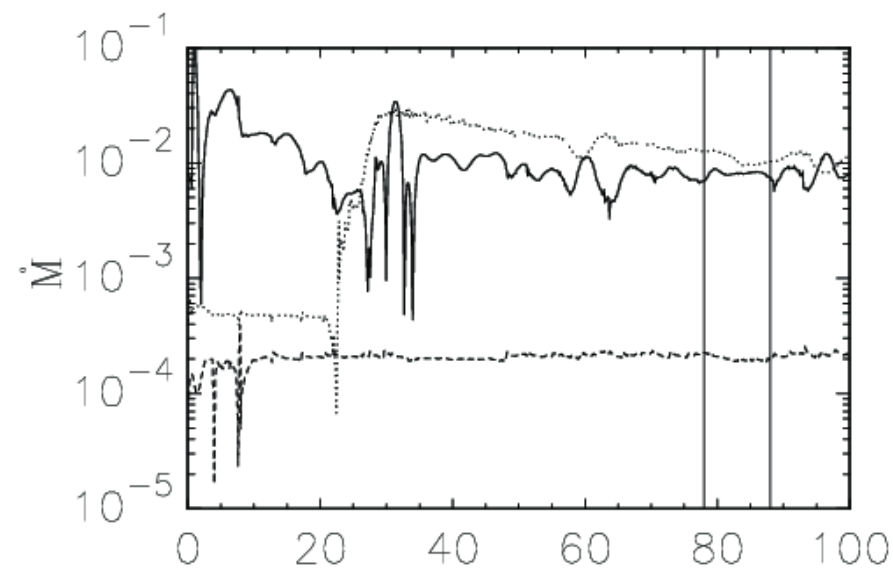


Time dependence of the mass and angular momentum fluxes in the various components in our simulations.

Star-disk magnetospheric interaction (SDMI) simulations

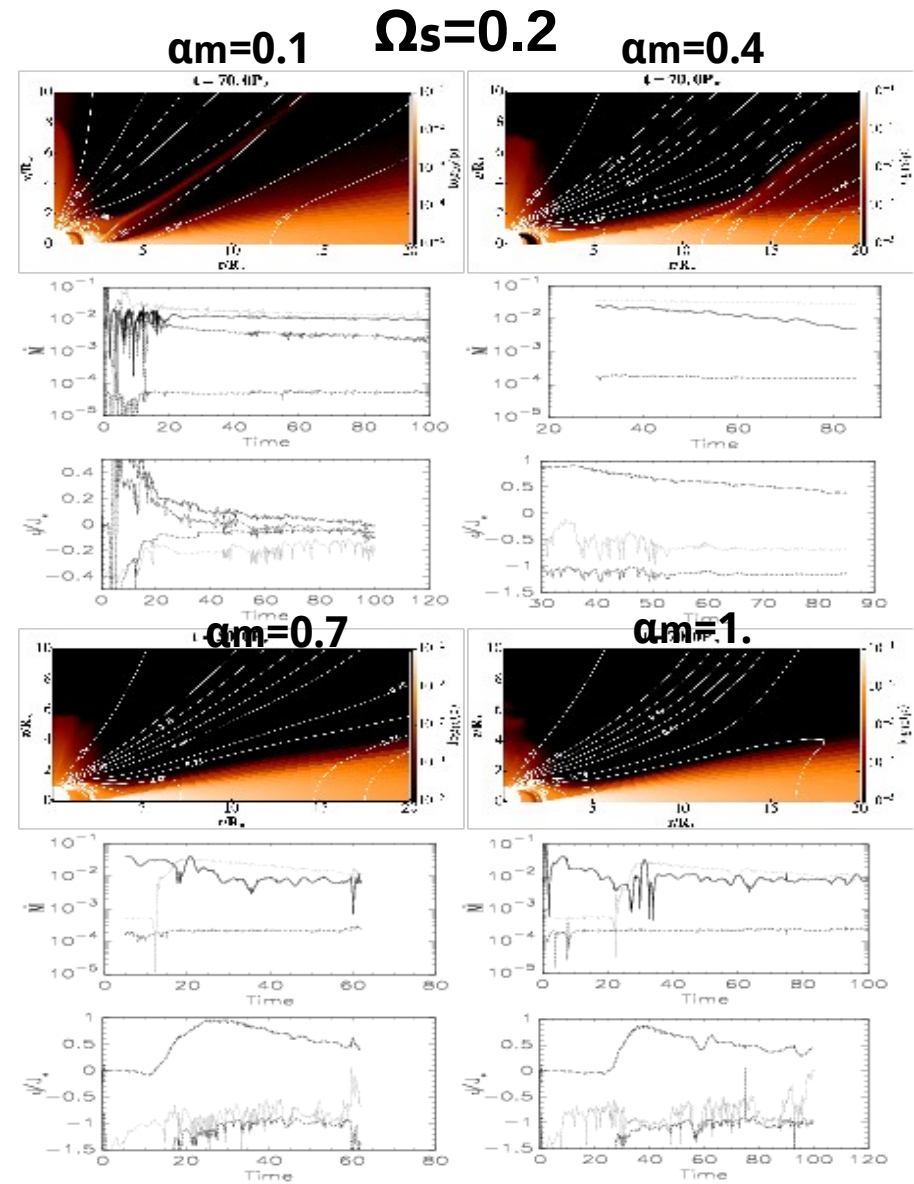
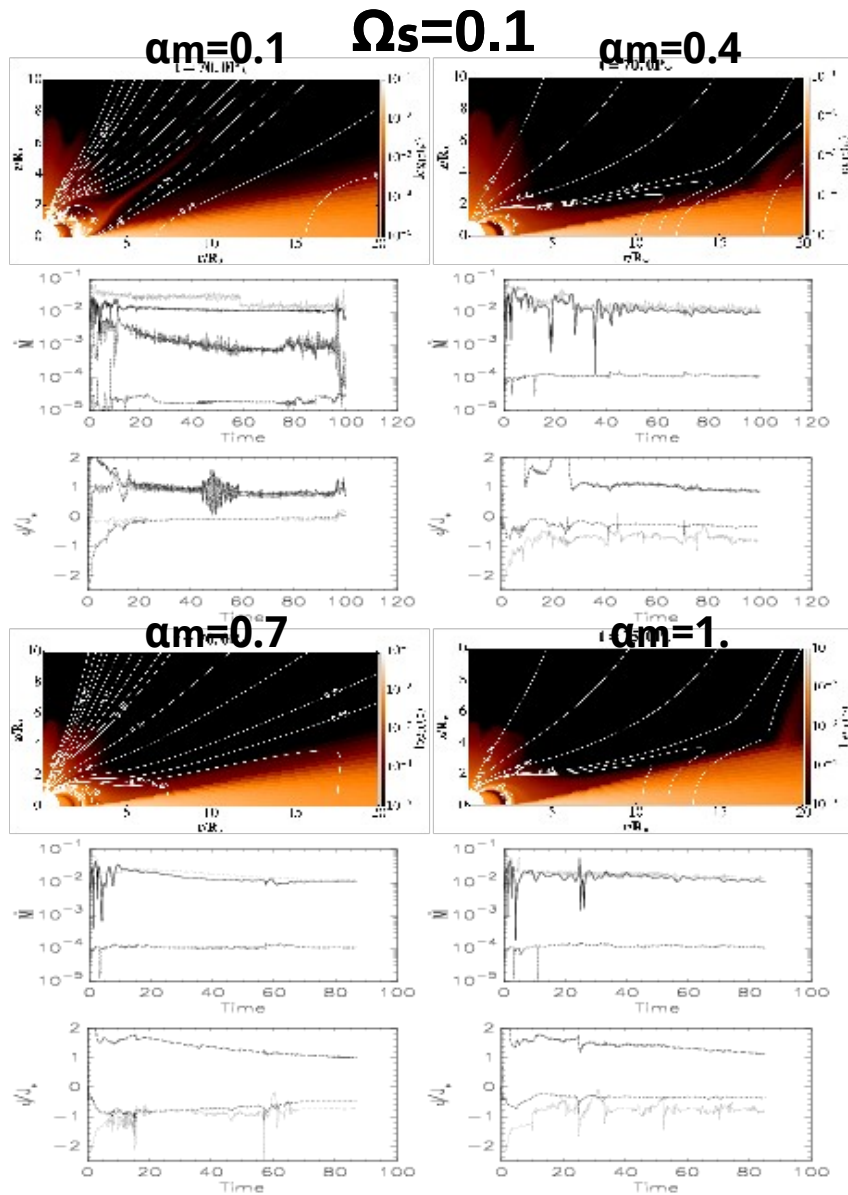


Computational box and a zoom closer to the star after 80 stellar rotations, to visualize the accretion column and the magnetic field lines (white solid lines), connected to the disk beyond the corotation radius $R_{\text{cor}} = 2.92 R_{\text{s}}$. In color is shown the density, and vectors show velocity, with the different normalization in the disk, column and stellar wind.

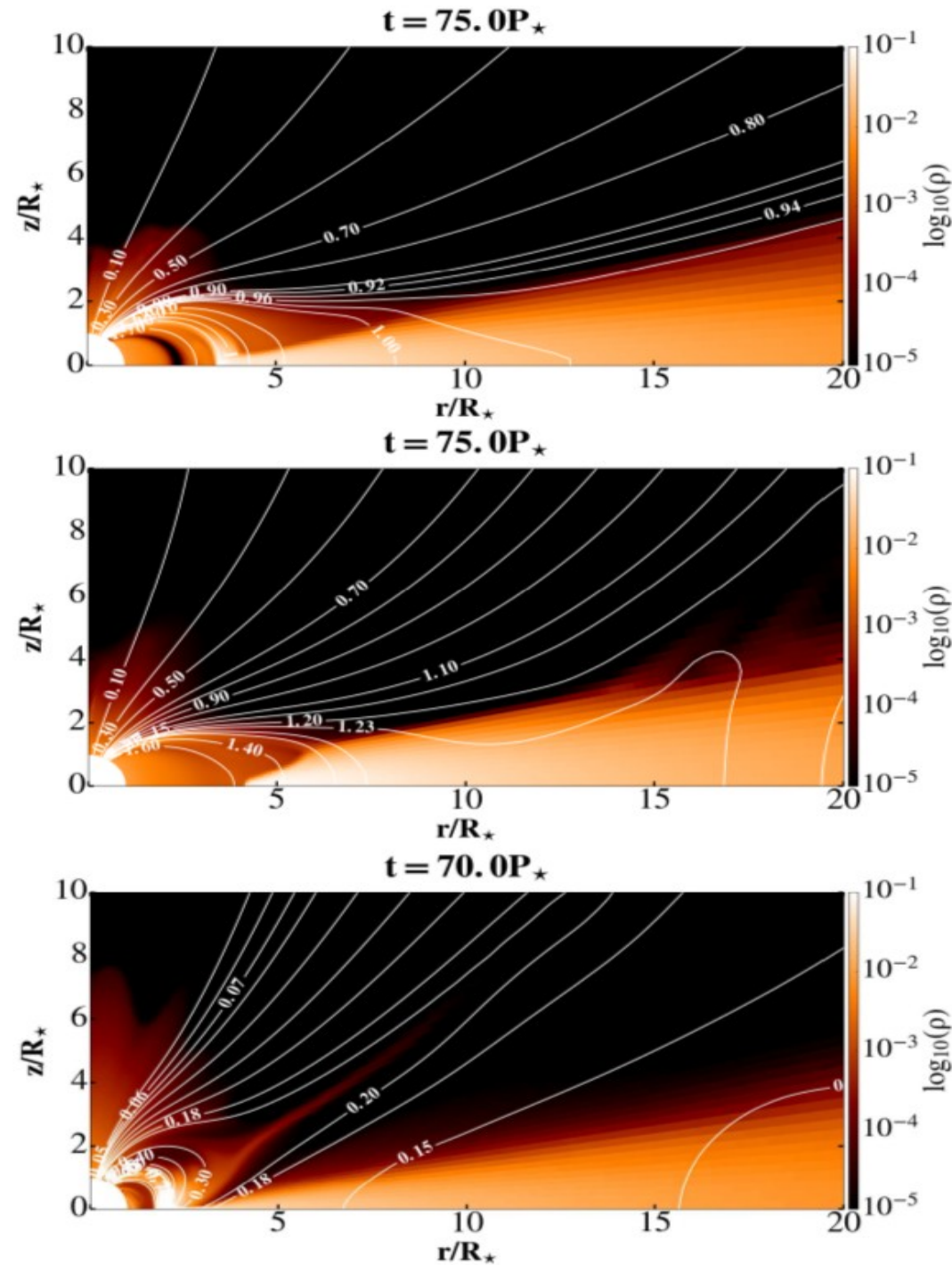


Time dependence of the mass and angular momentum fluxes in the various components in our simulations with marked the time interval in which the average for the quasi-stationarity is computed.

Part of the “Atlas” of solutions, with $B_s=500G$

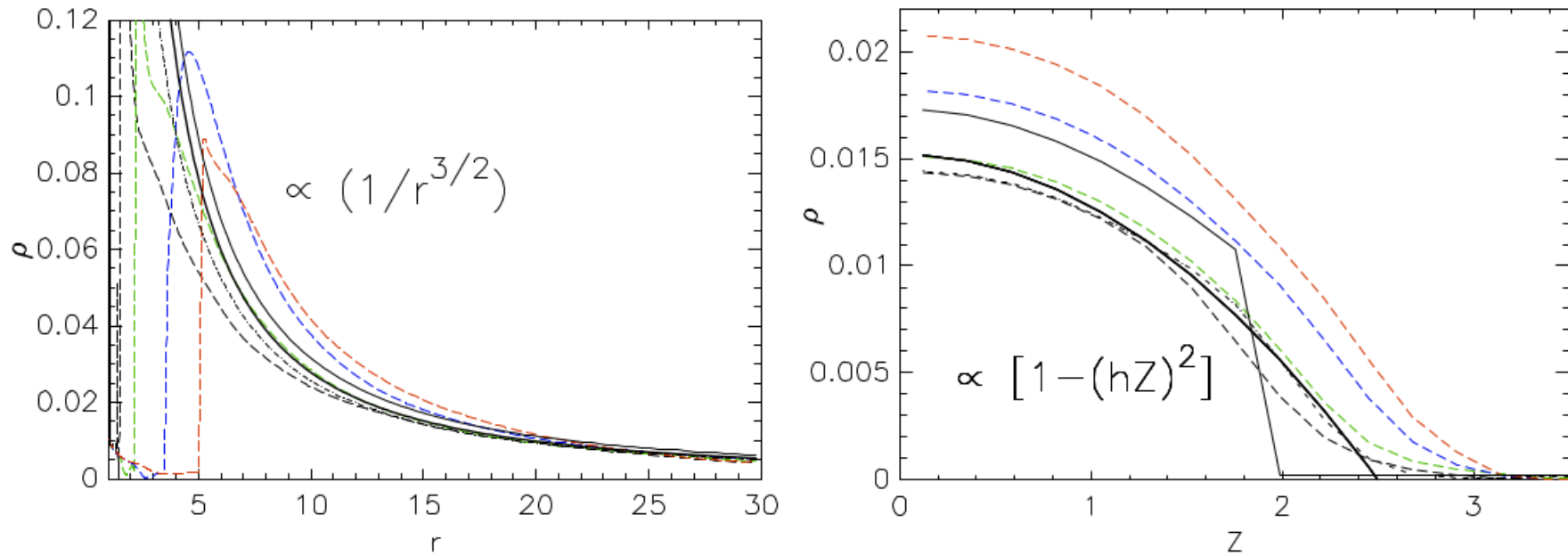


Configurations in “Atlas” solutions



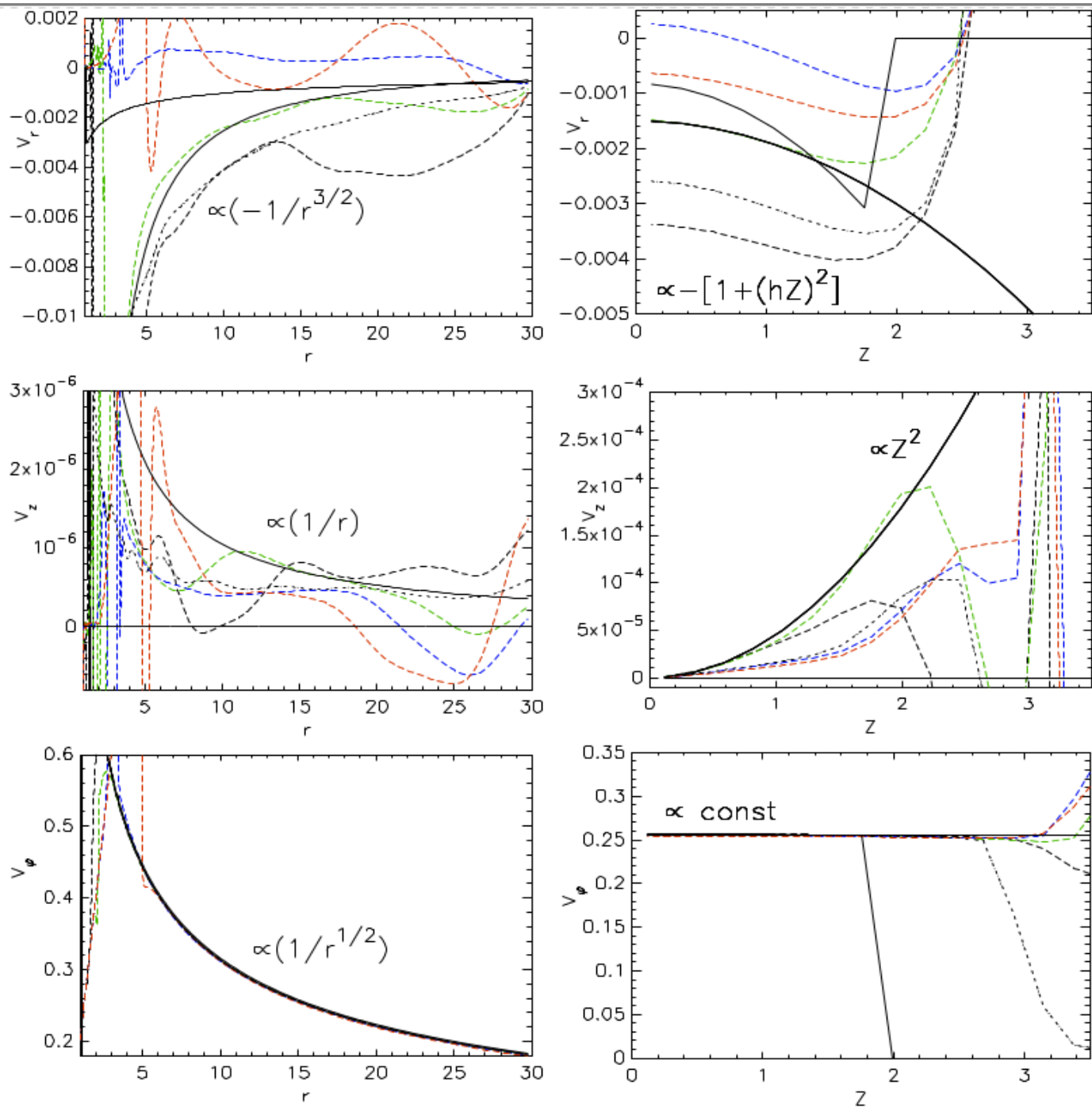
- There are three different cases of geometry in our results.
- In the top and middle panels are shown $B=1$ kG and the resistivity $\alpha_m=1$, in the cases with $\Omega_s=0.1$ (top panel) and $\Omega_s=0.15$ (middle panel).
- Faster stellar rotation prevents the accretion column formation.
- In the bottom panel is shown the third case, with $B=0.5$ kG, resistivity $\alpha_m=0.1$ and $\Omega_s=0.1$, where a conical outflow is formed.

Comparison of SDMI simulations with increasing mag. field



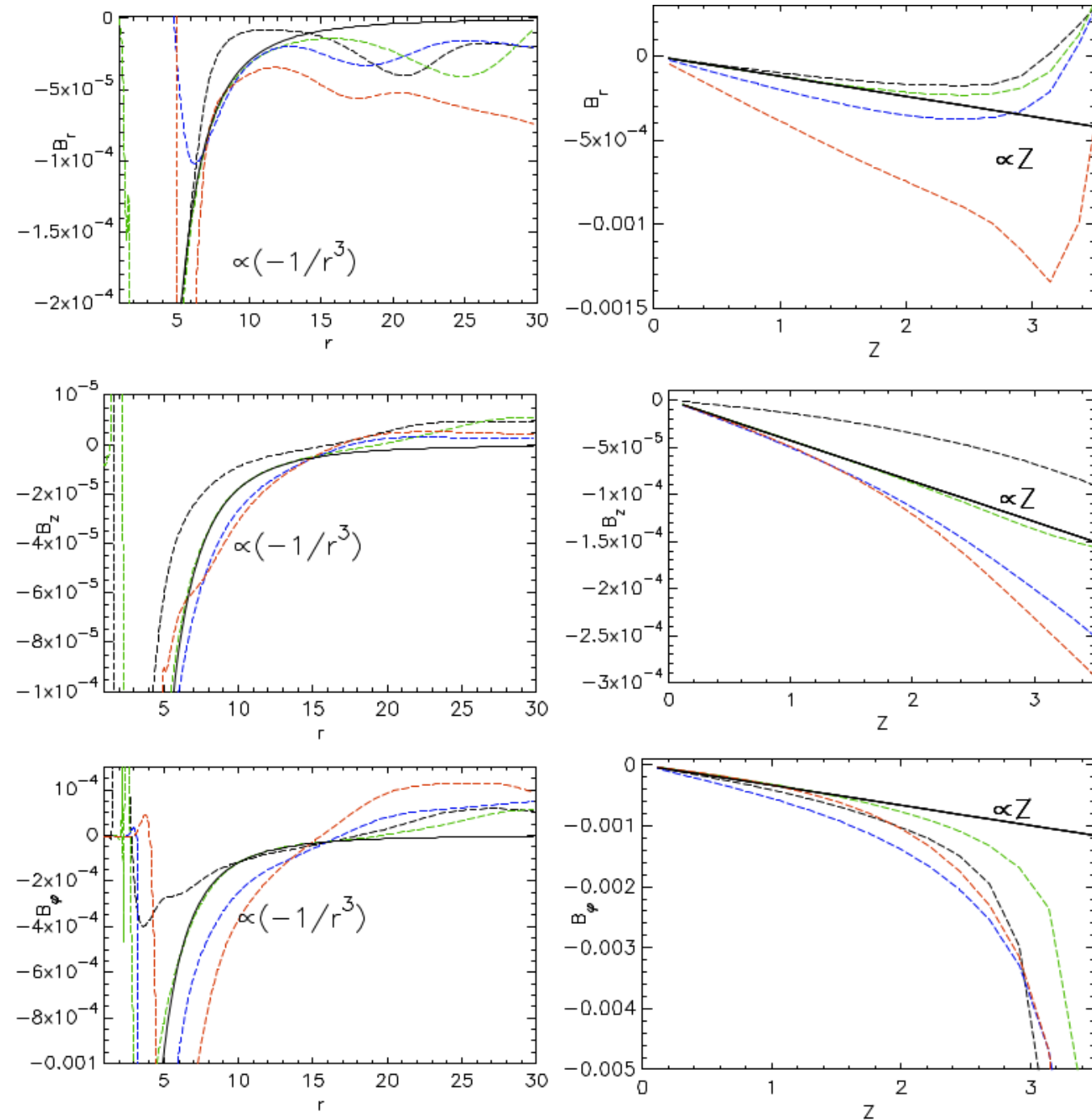
Comparison of the matter density in the initial set-up (thin solid line) with the quasi-stationary solutions in the numerical simulations in the HD (dot-dashed line) and the MHD (long-dashed line) cases. In black, green blue and red colors are the results in the MHD cases with the stellar magnetic field strength 0.25, 0.5, 0.75 and 1.0 kG, respectively. The closest fit to the 0.5 kG case is depicted with the thick solid line. In the left panel is shown the radial dependence nearby the disk equatorial plane, and in the right panel the profiles along the vertical line at $r=15$.

Comparison of SDMI simulations with increasing mag. field



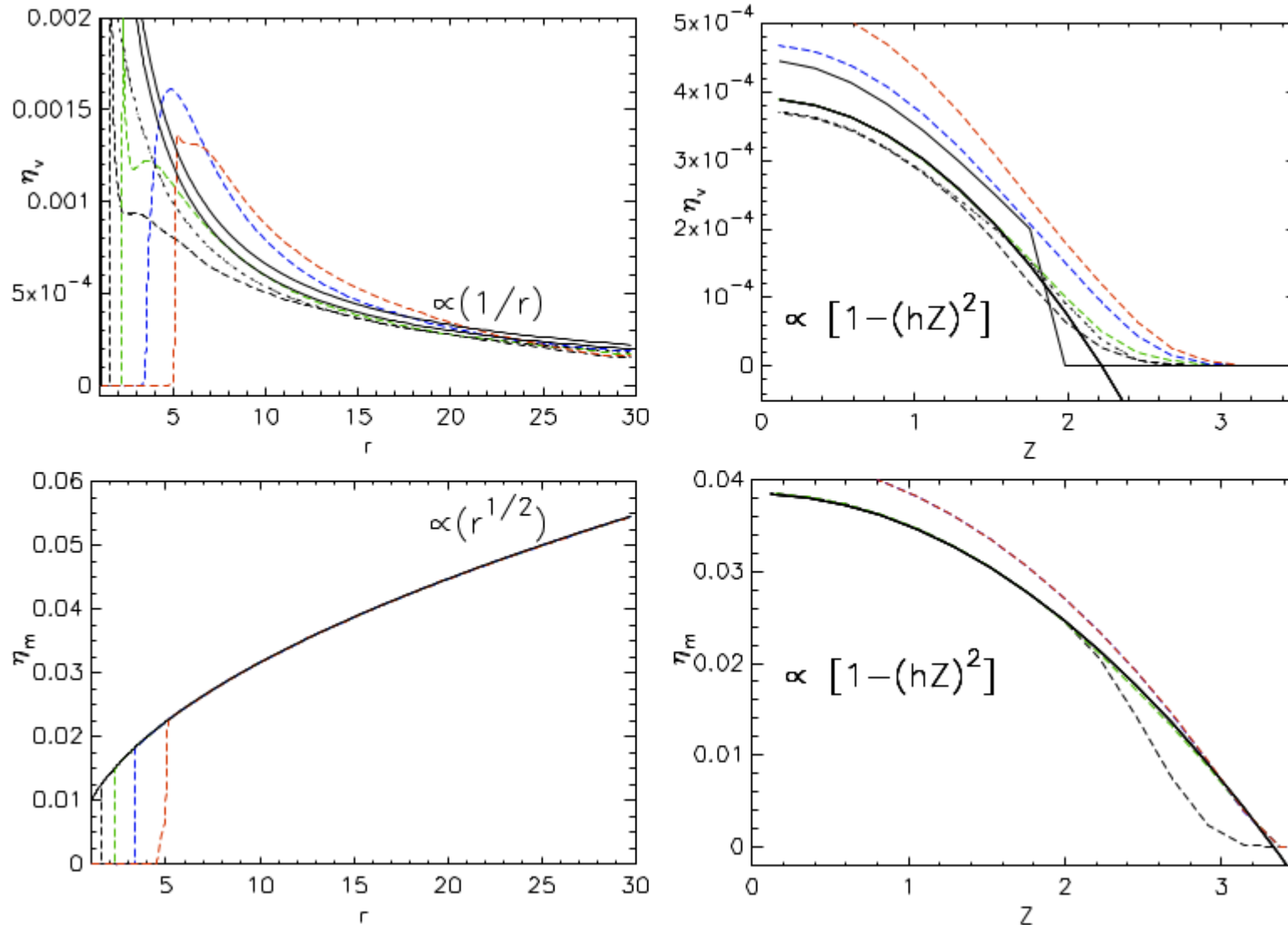
Comparison for velocities. In black, green blue and red colors are the results in the MHD cases with the stellar magnetic field strength 0.25, 0.5, 0.75 and 1.0 kG, respectively. The closest fit to the 0.5 kG case is depicted with the thick solid line.

Comparison of SDMI simulations with increasing mag. field



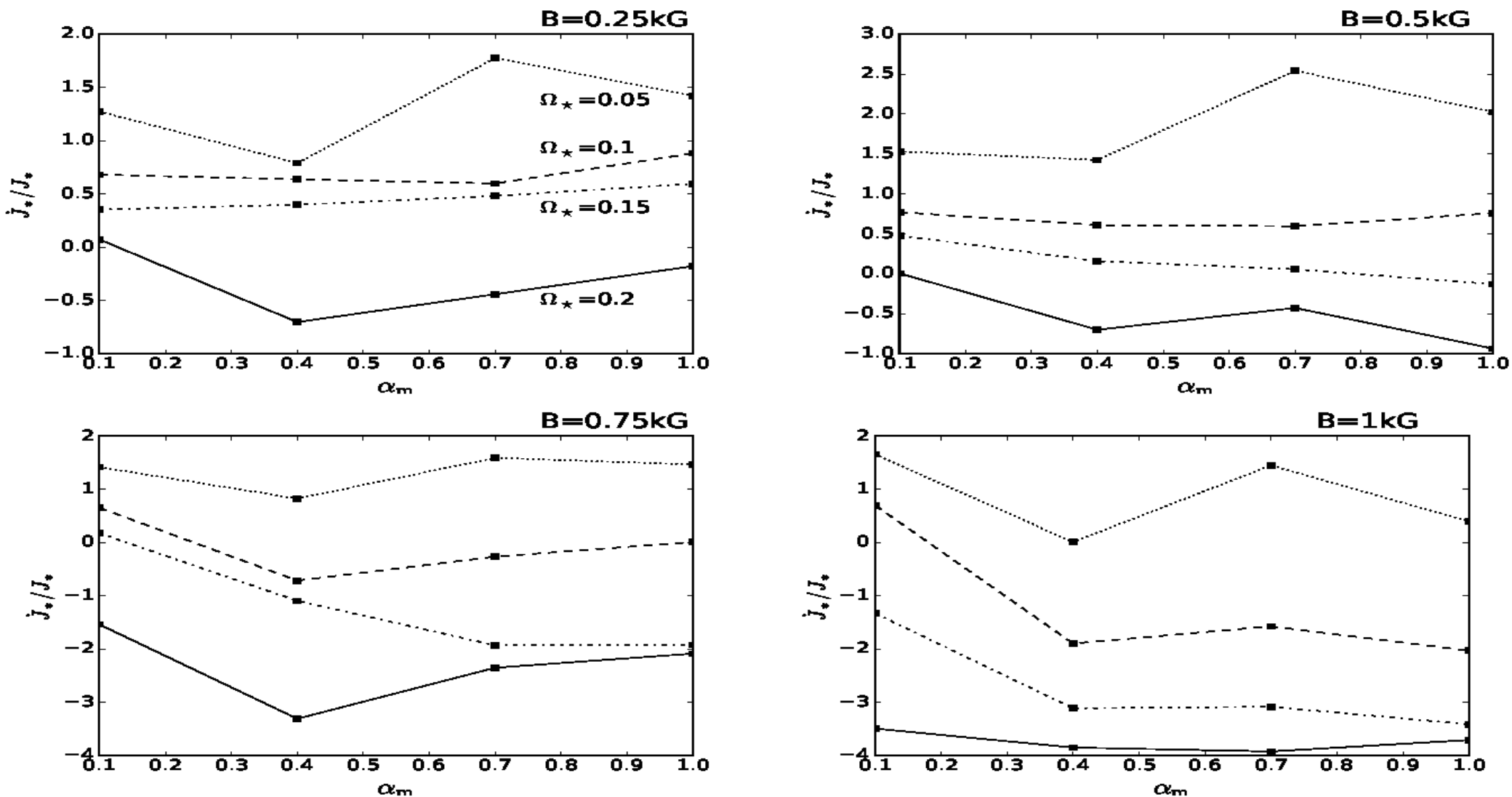
Comparison for magnetic field. In black, green blue and red colors are the results in the MHD cases with the stellar magnetic field strength 0.25, 0.5, 0.75 and 1.0 kG, respectively. The closest fit to the 0.5 kG case is depicted with the thick solid line.

Comparison of SDMI simulations with increasing mag. field



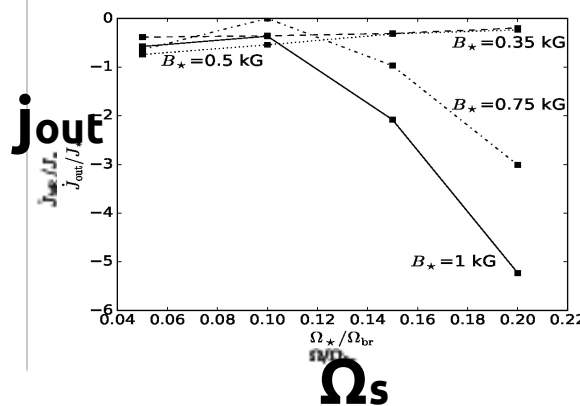
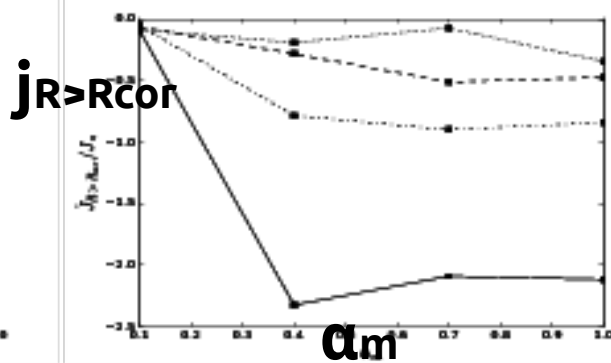
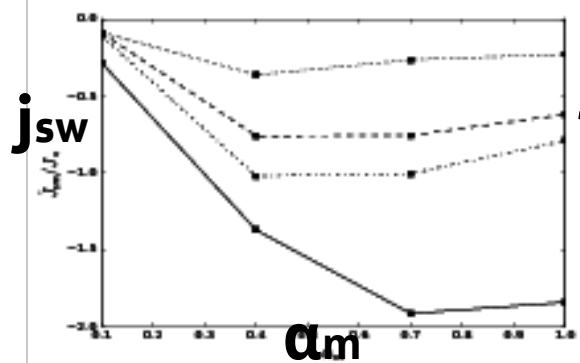
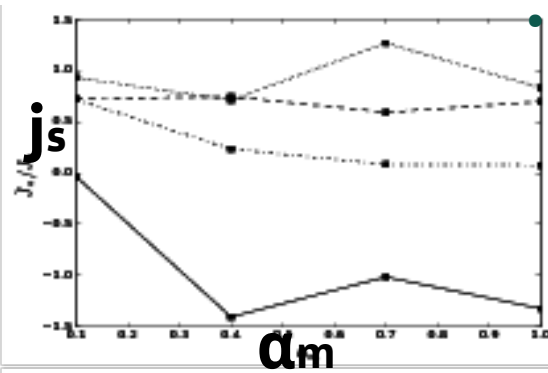
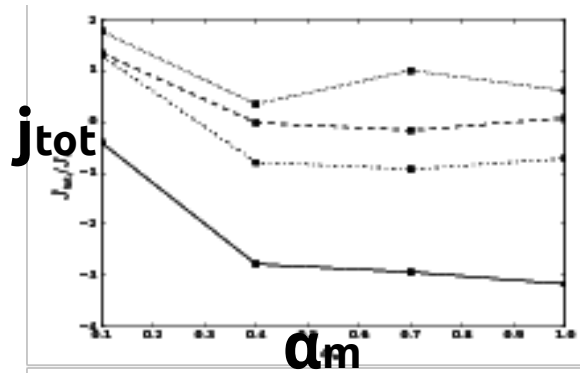
Comparison for diffusive coefficients. In black, green blue and red colors are the results in the MHD cases with the stellar magnetic field strength 0.25, 0.5, 0.75 and 1.0 kG, respectively. The closest fit to the 0.5 kG case is depicted with the thick solid line.

Trends in solutions with increasing stellar magnetic field



Average angular momentum flux transported onto the stellar surface by the matter in-falling from the disk onto the star through the accretion column. In each panel is shown a set of solutions with one stellar magnetic field strength, varying the stellar rotation rate and resistivity. Positive flux spins-up the star, negative slows it down. With the increase in stellar rotation rate, spin-up of the star by the infalling matter decreases, eventually switching to the spin-down.

Trends in the solutions with $B_s=0.5$ kG-preliminary results



Shown is the average angular momentum flux change with resistivity (α_m) in various components of the system, normalized to the stellar angular momentum. Dotted, dashed, dot-dashed and solid lines represent fluxes in $\Omega_s=0.05, 0.1, 0.15$ and 0.2 cases. We are interested in trends. Compared with observations, this can be used to improve the stellar models.

Angular momentum flux change with Ω_s , in all the cases with conical outflow (with $\alpha_m=0.1$), with different B_s .

Expressions for physical quantities in the disk

Table of proportionality coefficients in expressions for physical quantities in the disk.

h	B=500 G
h_1	0.88
h_2	0.087
h_3	0.003
h_4	0.255
h_5	0.405
h_6	0.145
h_7	1.114
h_8	0.006
h_9	0.01

$$\rho(r, z) = \frac{h_1}{r^{3/2}} [1 - (0.4z)^2],$$

$$v_r(r, z) = -\frac{h_2}{r^{3/2}} [1 + (0.5z)^2],$$

$$v_z(r, z) = \frac{h_3}{r} z^2,$$

$$v_\varphi(r, z) = \frac{h_4}{\sqrt{r}},$$

$$B_r(r, z) = -\frac{h_5}{r^3} z,$$

$$B_z(r, z) = -\frac{h_6}{r^3} z,$$

$$B_\varphi(r, z) = -\frac{h_7}{r^2} z,$$

$$\eta(r, z) = \frac{h_8}{r} [1 - (0.45z)^2],$$

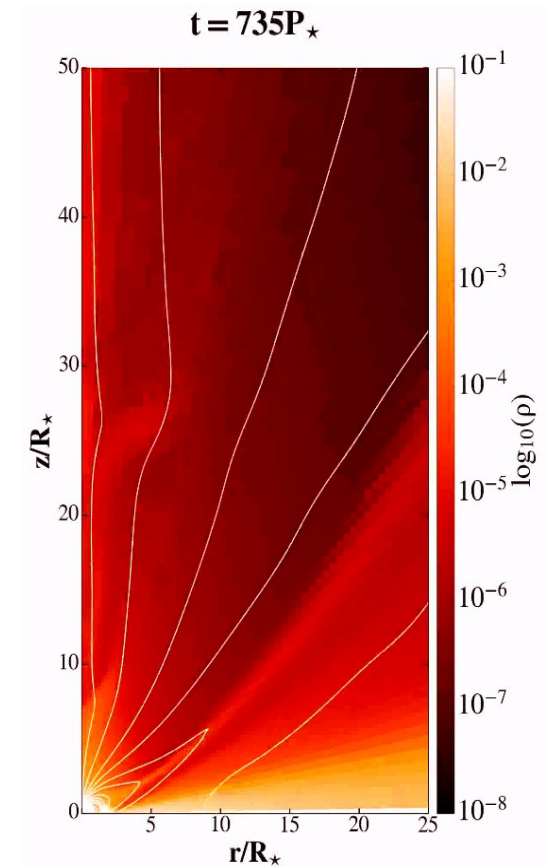
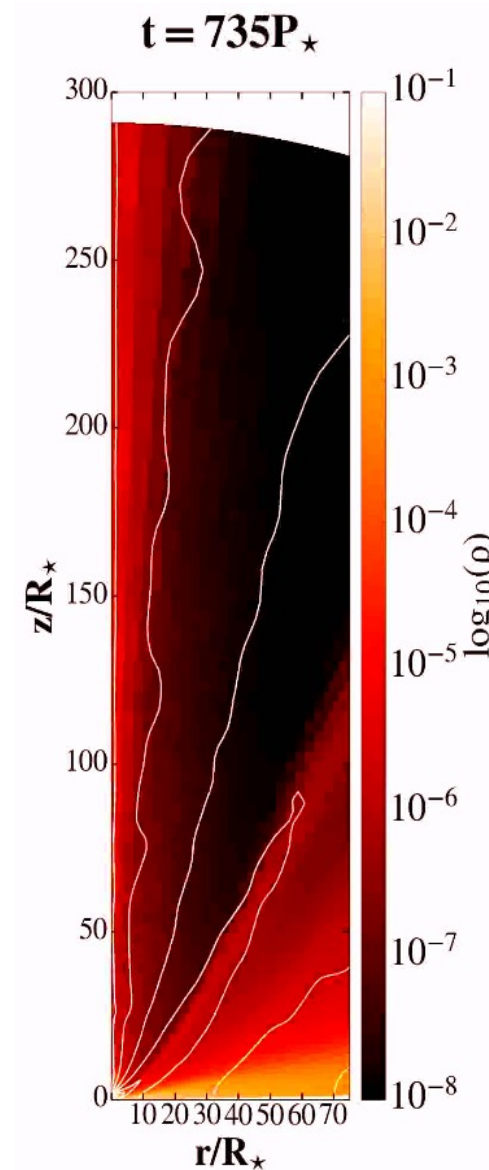
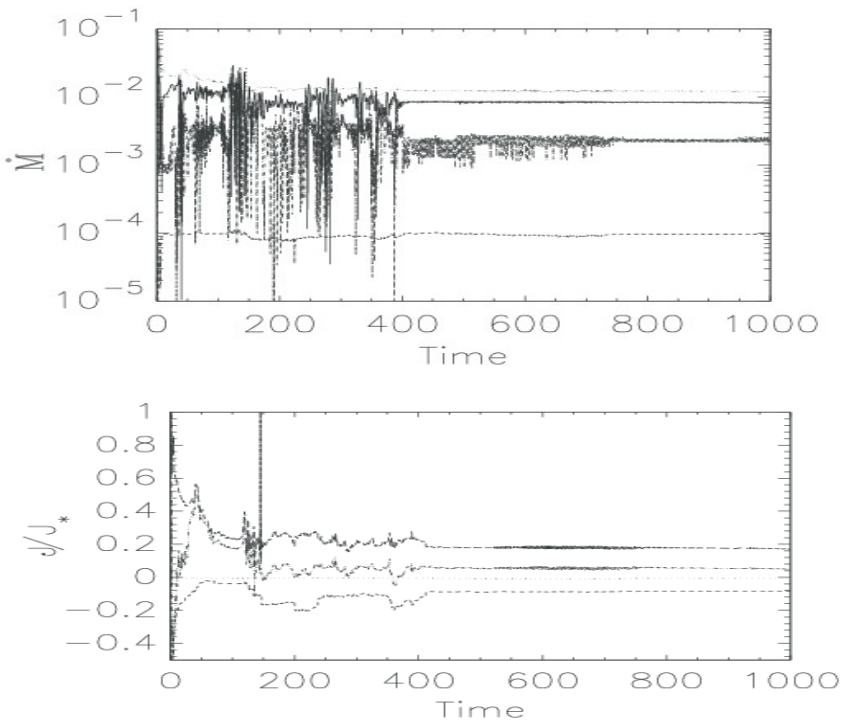
$$\eta_m(r, z) = h_9 \sqrt{r} [1 - (0.3z)^2].$$

*Expressions for physical quantities in the disk.
h are the proportionality factors of fitting curves.*

Jet launching

In the cases with faster stellar rotation, I obtained a continuous launching of an axial jet from the star-disk magnetosphere.

The axial jet and the conical outflow are similar to the results in Romanova et al. (2009) and Zanni & Ferreira (2013).



Zoom into the launching region.

Summary

- I obtained viscous and resistive MHD star-disk magnetospheric interaction solutions for a thin accretion disk.
- A quasi-stationary state is obtained in a set of 64 simulations with slowly rotating stars.
- Results are compared, to find trends in solutions.
- In the cases with $\alpha_m=0.1$, a conical outflow is launched.
- In the cases with faster rotating stars than those in our parameter study, an axial jet is launched.